Inorganic Chemistry

Article

Lithium-Alkyl, -Aryl, and -Amido Ligand-Exchange Dynamics of Dianionic Zirconium(IV) Complexes with Chelating Amidophenolate Ligands

Karen J. Blackmore, Joseph W. Ziller, and Alan F. Heyduk*

Department of Chemistry, University of California, Irvine, California 92697

Received June 6, 2007

The synthesis, characterization, and solution behavior of a series of six-coordinate zirconium(IV) dianions [ZrX$_2$(ap)$_2$]$^{2-}$ (ap = 2,4-di-*tert*-butyl-6-(*tert*-butylamido)phenolate; X = Ph, **3a**; X = *p*-tolyl, **3b**; X = Me, **4**; X = NMe$_2$, **5**) are described. Complexes **3**–**5** were prepared by treating the neutral zirconium complex Zr(ap)$_2$(THF)$_2$ (**1**) with 2 equiv of LiX or by the direct reaction of apLi$_2$ and LiX with ZrCl$_4$. The complexes were isolated as lithium-etherate salts, and they were characterized by NMR spectroscopy and single-crystal X-ray diffraction. In non-coordinating solvents such as benzene-*d*$_6$, complexes **3**–**5** are robust in solution, but in coordinating solvents such as THF-*d*$_8$, dissociation of LiX was observed. The rate of LiX loss was evaluated by exchange reactions; the reaction rate constants span nine orders of magnitude at 298 K, with the slowest reaction being the dissociation of PhLi from **3a** ($\tau_{1/2}$ = 4 h) and the fastest reaction being the dissociation of LiNMe$_2$ from **5** ($\tau_{1/2}$ = 53 μs). In the case of LiNMe$_2$ dissociation from **5**, activation parameters suggest that the rate-determining step is purely dissociative; however, for diphenyl and dimethyl complexes **3a** and **4**, respectively, activation parameters suggest a solvent-assisted rate-determining step.

Introduction

The exchange of ligands at transition metal centers is a fundamental process that must be understood to design catalysts for small molecule transformations. In particular, the exchange of alkyl, aryl, amide, alkoxide, and halide ligands is critical to the success of reactions that form new X−X or X−Y bonds. For early transition metal complexes, the most notable ligand exchange studies involve the abstraction of anionic alkyl or halide ligands to generate electrophilic transition metal cations for olefin polymerization.[1−4] In these studies, the mechanism of methyl and halide abstraction has been probed to understand better the amount of active catalyst species, the rate of its generation, and its lifetime in the reaction.

Our interest in understanding the ligand exchange dynamics of Group IV metal complexes stems from studies of new bond-forming and bond-cleaving reactions that involve redox-active catecholate-type ligands. Recently, we reported an oxidative-addition-like reaction in which 2,4-di-*tert*-butyl-6-(*tert*-butylamido)phenolate ligands (ap^{2-}), provide the reducing equivalents for halogen addition to a d^0, zirconium-(IV) metal center (Scheme 1a).[5] The reverse reaction, reductive elimination enabled by ligand-based redox equivalents, was realized for a diphenyl zirconium complex. As shown in Scheme 1b, two-electron oxidation of the zirconium(IV) dianion, [ZrPh$_2$(ap)$_2$]$^{2-}$, affords a putative diphenyl intermediate that rapidly reacts by a unimolecular C−C bond-forming pathway to extrude biphenyl.[6] In this reaction, the redox-active ligands work as an electron reservoir to accept two electrons upon elimination of the biphenyl C−C bond.
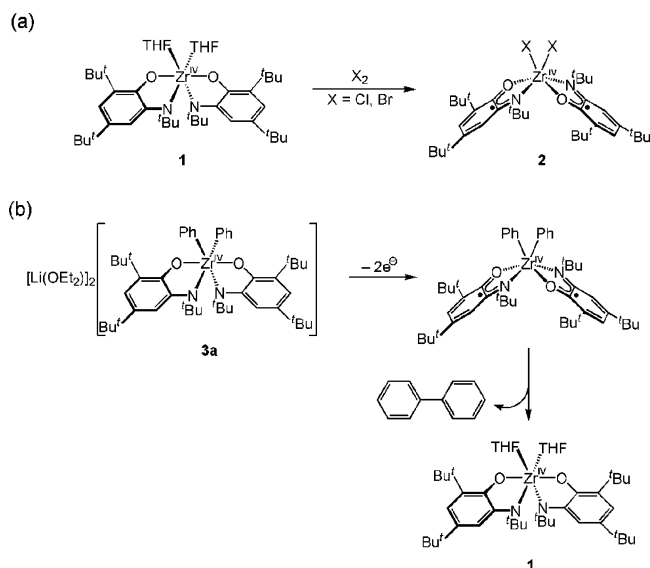
While oxidation-induced reductive elimination from **3a** to form a biphenyl-type product is facile, the analogous reaction to couple sp^3-hybridized methyl ligands is problematic. Two-electron oxidation of [ZrMe$_2$(ap)$_2$]$^{2-}$ affords products consistent with both unimolecular, reductive-elimination and bimolecular, radical reaction pathways. We suspected that

* To whom correspondence should be addressed. E-mail: aheyduk@ uci.edu.

(1) (a) Chen, E. Y. X.; Marks, T. J. *Chem. Rev.* **2000**, *100*, 1391−1434; (b) Yang, X.; Stern, C. L.; Marks, T. J. *J. Am. Chem. Soc.* **1991**, *113*, 3623−3625; (c) Yang, X.; Stern, C. L.; Marks, T. J. *J. Am. Chem. Soc.* **1994**, *116*, 10015−10031.
(2) Kaminsky, W.; Steiger, R. *Polyhedron* **1988**, *7*, 2375−2381.
(3) Breslow, D. S.; Newburg, N. R. *J. Am. Chem. Soc.* **1959**, *81*, 81−86.
(4) Chien, J. C. W. *J. Am. Chem. Soc.* **1959**, *81*, 86−92.

(5) Blackmore, K. J.; Ziller, J. W.; Heyduk, A. F. *Inorg. Chem.* **2005**, *44*, 5559−5561.
(6) Haneline, M. R.; Heyduk, A. F. *J. Am. Chem. Soc.* **2006**, *128*, 8410− 8411.

Scheme 1

(a)

(b)

the desired oxidation-induced reductive-elimination chemistry was being circumvented by a faster ligand exchange processes at the $[ZrX_2(ap)_2]^{2-}$ dianion.[7,8]

In this paper, we report the results of ligand exchange studies on dianionic zirconium(IV) complexes with the general formula $[ZrX_2(ap)_2]^{2-}$ (**3a**, X = Ph; **3b**, X = *p*-tolyl; **4**, X = Me; **5**, X = NMe$_2$). In these complexes, four zirconium coordination sites are taken up by strongly binding amidophenolate ligands, leaving two sites for the binding of monodentate, monoanionic donor ligands. These monoanionic ligands exchange from the zirconium center as LiX by a dissociative mechanism at rates that vary dramatically with the identity of the X group. While PhLi dissociation from **3a** is very slow ($\tau_{1/2}$ = 4 h at 298 K), MeLi exchange from **4** is faster by a factor of 10^2. The dissociation of LiNMe$_2$ from **5** is over nine orders of magnitude faster than PhLi exchange from **3a**, with a room-temperature half-life of 53 μs. This manuscript reports the synthesis, structures, and solution dynamic behavior of zirconium(IV) complexes of the general formula $[ZrX_2(ap)_2]^{2-}$.

Experimental Section

General Experimental Considerations. The complexes described below are extremely air and moisture sensitive. All manipulations were carried out under an atmosphere of argon or nitrogen gas using standard Schlenk, vacuum-line, and glovebox techniques. High-purity solvents were first sparged with argon and then purified dried by passage through activated alumina and Q5 columns to remove water and oxygen, respectively. The metal salt ZrCl$_4$ was purchased from Alfa-Aesar and used as received. Lithium dimethylamide and methyl-d_3-lithium were purchased from Aldrich

(7) Typically, reductive elimination of sp^2-hybridized centers proceeds faster that the reductive elimination of sp^3-hybridized centers thanks to better orbital overlap in the transition state, see Collman, J. P.; Hegedus, L. S.; Norton, J. R.; Finke, R. G. *Principles and Applications of Organotransition Metal Chemistry*, 2nd ed.; University Science Books: Mill Valley, CA, 1987; Section 5.6.

(8) On the other hand, differences in the oxidation-induced reactivity of Cp$_2$ZrMe$_2$ and Cp$_2$ZrPh$_2$ have been attributed to inherent differences in the Zr−C bond strength. See Borkowsky, S. L.; Jordan, R. F.; Hinch, G. D. *Organometallics* **1991**, *10*, 1268−1274.

and used as received. The 2,4-di-*tert*-butyl-6-(*tert*-butylamino)-phenol ligand (apH$_2$) was prepared by a previously reported procedure.[5] The zirconium complexes, Zr(ap)$_2$(THF)$_2$ (**1**), [Li-(OEt$_2$)]$_2$[ZrPh$_2$(ap)$_2$] (**3a**), [Li(OEt$_2$)]$_2$[Zr(*p*-tolyl)$_2$(ap)$_2$] (**3b**), and [Li(OEt$_2$)]$_2$[ZrMe$_2$(ap)$_2$] (**4**), have been previously reported,[5,6] but ^{1}H NMR spectra in benzene-d_6 and THF-d_8 are included in the Supporting Information for direct comparison purposes.

All complexes were characterized by ^{1}H and ^{13}C NMR spectroscopy, IR spectroscopy, and elemental analysis. NMR spectra were collected on Bruker Avance 500 or 600 MHz spectrometers in either benzene-d_6 or THF-d_8 solvents that were degassed by several freeze−pump−thaw cycles, dried over sodium benzophenone ketyl radical, and vacuum-distilled before use. ^{1}H and ^{13}C NMR spectra were referenced to TMS using the residual ^{1}H and natural abundance ^{13}C impurities, respectively, of the solvent. All chemical shifts are reported using the standard δ notation in ppm. Infrared spectra were recorded on a Perkin-Elmer Spectrum One spectrophotometer as KBr pellets. Elemental analyses were provided by Desert Analytics.

Preparation of [Li(OEt$_2$)]$_2$[Zr(NMe$_2$)$_2$(ap)$_2$] (5). In a 20 mL scintillation vial, a 10 mL ether solution containing 3.60 mmol of apLi$_2$ (2 equiv, prepared in situ from 1.00 g of apH$_2$ and 2.88 mL of 2.5 M *n*-butyllithium) was frozen in a liquid-nitrogen cold well. Immediately upon thawing, the apLi$_2$ mixture was added to a stirring suspension of 0.42 g of ZrCl$_4$ (1.80 mmol, 0.5 equiv) in cold ether (3 mL), followed by the addition of 0.18 g of solid lithium dimethylamide (3.6 mmol, 2 equiv). The reaction mixture was allowed to warm to 26 °C and was stirred overnight, affording an orange solution with a white precipitate. Filtration and solvent removal gave an orange residue that was triturated with pentane (3 × 10 mL) and then cooled to −35 °C. Collection of the yellow crystals gave 0.25 mg of **5** (32% yield). X-ray quality crystals of **5** were obtained by chilling saturated pentane solutions of the complex to −35 °C. Anal. Calcd for C$_{48}$H$_{90}$Li$_2$N$_4$O$_4$Zr: C, 64.61; H, 10.17; N, 6.28. Found: C, 64.5; H, 9.95; N, 5.97. ^{1}H NMR (600 MHz, C$_6$D$_6$) δ/ppm: 0.73 (*t*, 12H, EtOCH$_2$C*H$_3$*, $^3J_{HH}$ = 7.0 Hz), 1.41 (*s*, 18H, C(C*H$_3$*)$_3$), 1.56(*s*, 18H, C(C*H$_3$*)$_3$), 1.82 (*s*, 18H, C(C*H$_3$*)$_3$), 2.88 (*q*, 8H, EtOC*H$_2$*CH$_3$, $^3J_{HH}$ = 7.0 Hz), 3.16 (*s*, 12H, N(C*H$_3$*)$_2$), 6.85 (*d*, 2H, aryl-*H*, $^3J_{HH}$ = 1.9 Hz), 6.90 (*d*, 2H, aryl-*H*, $^3J_{HH}$ = 1.9 Hz). ^{13}C NMR (125.8 MHz, C$_6$D$_6$) δ/ppm: 14.1 (EtOCH$_2$*C*H$_3$), 30.9 (C(*C*H$_3$)$_3$), 30.9 (C(*C*H$_3$)$_3$), 32.4 (C(*C*H$_3$)$_3$), 34.7 (*C*(CH$_3$)$_3$), 35.2 (*C*(CH$_3$)$_3$), 46.1 (N(*C*H$_3$)$_2$), 53.5 (N*C*(CH$_3$)$_2$), 65.6 (EtO*C*H$_2$CH$_3$), 109.9 (aryl-*C*), 111.7 (aryl-*C*), 133.7 (aryl-*C*), 138.9 (aryl-*C*), 147.6 (aryl-*C*), 152.9 (aryl-*C*).

General Crystallographic Procedures. X-ray diffraction data for **5** were collected for a yellow crystal of approximate dimensions 0.20 × 0.24 × 0.42 mm^3 mounted on a glass fiber with a Bruker CCD platform diffractometer equipped with a CCD detector. Measurements were carried out at 163 K using Mo Kα (λ = 0.71073 Å) radiation, which was wavelength selected with a single-crystal graphite monochromator. The SMART[9] program package was used to determine unit-cell parameters and to collect data (25 s/frame scan time for a sphere of diffraction data). The raw frame data were processed using SAINT[10] and SADABS[11] to yield the reflection data files. Subsequent calculations were carried out using the SHELXTL program suite.[12] The diffraction symmetry was

(9) *SMART*, Version 5.1; Bruker Analytical X-Ray Systems, Inc.: Madison, WI, 1999.

(10) *SAINT*, Version 5.1; Bruker Analytical X-Ray Systems, Inc.: Madison, WI, 1999.

(11) Sheldrick, G. M. *SADABS*, Version 2.05; Bruker Analytical X-Ray Systems, Inc.: Madison, WI, 2001.

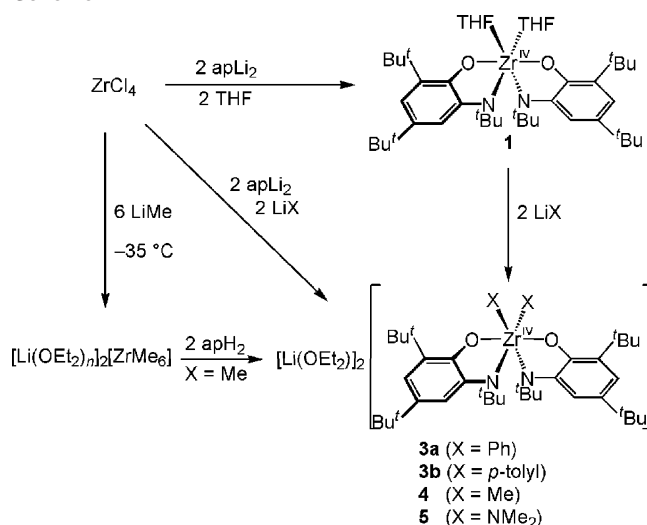(12) Sheldrick, G. M. *SHELXTL*, Version 6.12; Bruker Analytical X-Ray Systems, Inc.: Madison, WI, 2001.

Table 1. Crystal Data Collection and Refinement Parameters for [Li(OEt$_2$)]$_2$[Zr(NMe$_2$)$_2$(ap)$_2$] (**5**)

empirical formula	C$_{48}$H$_{90}$Li$_2$N$_4$O$_4$Zr
fw	892.34
cryst syst	orthorhombic
space group	*Pbcn*
a/Å	17.682(2)
b/Å	17.923(2)
c/Å	16.4037(19)
V/Å^3	5198.6(10)
Z	4
reflns collected	51 186
independent reflns	5729
GOF	1.063
R1 [$I > 2\sigma(I) = 4640$ data]	0.0486
wR2 (all data; 0.78 Å)	0.1298

mmm, and the systematic absences were consistent with the orthorhombic space group *Pbcn* that was later determined to be correct. The structure was solved by direct methods and refined on F^2 by full-matrix least-squares techniques. Analytical scattering factors for neutral atoms were used throughout the analyses.[13] Hydrogen atoms were included using a riding model. The molecule was located on a 2-fold rotation axis. Carbon atoms C(23) and C(24) were disordered and included using multiple components, partial site-occupancy-factors and isotropic thermal parameters. ORTEP diagrams were generated using ORTEP-3 for Windows.[14] Diffraction data for **5** are shown in Table 1.

Kinetic Studies of 5. The rate of LiNMe$_2$ exchange at **5** was sufficiently fast that it was monitored by variable-temperature ^{1}H NMR spectroscopy. An NMR tube fitted with a J.Young Teflon valve was filled with 24 mg of **5** and 1 mg of LiNMe$_2$. THF-d_8 was added to the tube by vacuum-transfer, and both reagents dissolved. ^{1}H NMR spectra (500 MHz) were recorded on the sample between 248 and 308 K. At each temperature, the sample was allowed to equilibrate for 5 min before data collection began. Rate constants were extracted from the observed coalescence of the dimethylamide peaks by fitting the spectral data according to the complete band shape method.[15] Activation parameters for the exchange process were extracted from an Eyring plot over the entire temperature range.

Kinetic Studies of 3a and 4. The exchange of free and coordination PhLi from **3a** was investigated using traditional kinetics techniques. In a typical kinetics experiment, 20 mg of **3a** and 400 μL of THF-d_8 were added to a screw-capped NMR tube equipped with a Teflon-lined septum. In a separate vial, 10 equiv of *p*-tolyl lithium and 8 equiv of phenyllithium were dissolved in 200 μL of THF-d_8. Both solutions sat for 1 h before the experiment began. The NMR tube containing **3a** was inserted in the spectrometer, and the system temperature was allowed to equilibrate for 10 min. Immediately before data collection, the sample was ejected and the solution containing *p*-tolylLi and PhLi was added to the tube with a gas-tight microsyringe. The sample was shaken briefly and reinserted into the spectrometer. The reaction was followed to equilibrium by monitoring the decay of **3a** by ^{1}H NMR spectroscopy. The order of the reaction with respect to [**3a**], [PhLi], and [*p*-tolylLi] was determined from concentration-dependence studies. Temperature-dependence rate experiments between 298 and 338 K were used to construct an Eyring plot and extract activation parameters.

(13) *International Tables for X-Ray Crystallography*; Kluwer Academic Publishers: Dordrecht, The Netherlands, 1992; Vol. C.
(14) Farrugia, L. J. *J. Appl. Cryst.* **1997**, *30*, 565.
(15) Sandstrom, J. *Dynamic NMR Spectroscopy*; Academic Press, Inc.: New York, 1982.

Scheme 2

An analogous experimental protocol was used to probe the exchange of free and coordinated MeLi from **4**. In the case of diphenyl derivative **4**, the rate of ligand exchange was monitored by treating **4** with 10 equiv of CD$_3$Li and 8 equiv of CH$_3$Li. The temperature dependence of the exchange rate was determined between 268 and 308 K to give activation parameters, while concentration dependencies were used to determine the rate law for the reaction.

Results

Synthesis and Solid-State Characterization of Zirconium Amidophenolate Mono- and Dianions. Stable dianionic zirconium(IV) complexes with terminal phenyl, methyl, and dialkylamide ligands are readily supported by the chelating ap^{2-} ligand. The neutral form of this ligand, apH$_2$, was isolated from the condensation of ^{t}BuNH$_2$ with 3,5-di-*tert*-butylcatechol after a reductive workup. Deprotonation of apH$_2$ with *n*BuLi afforded apLi$_2$, which reacted with ZrCl$_4$-(THF)$_2$ to form the neutral, six-coordinate zirconium(IV) complex **1** in high yields as a yellow microcrystalline solid (Scheme 2). While **1** forms a distorted octahedral complex with two coordinated THF molecules in the solid state, the ^{1}H NMR spectrum of **1** in THF-d_8 showed that the coordinated solvent molecules exchanged rapidly in solution. This result suggested that the labile THF ligands may be displaced by other two-electron donors, prompting an investigation of alkyl, aryl, and amide ligands. The addition of excess PhLi to ether solutions of **1** at 25 °C resulted in a color change from pale yellow to red. The reaction product, **3a**, was isolated by recrystallization at low temperatures. A more convenient route to **3a** was the direct reaction of ZrCl$_4$ with 2 equiv each of apLi$_2$ and PhLi, which afforded the product in 65% yield. As shown in Scheme 2, both routes proved suitable for the synthesis of a variety of analogs to **3a** discussed in this manuscript, including the bis(*p*-tolyl) complex, **3b**, the dimethyl complex, **4**, and the bis(dimethylamide) complex, **5**, in yields ranging from 32% to 73%.

Compounds **3a**, **4**, and **5** have been characterized by single-crystal X-ray diffraction methods in the solid state where the zirconium(IV) centers are six-coordinate with
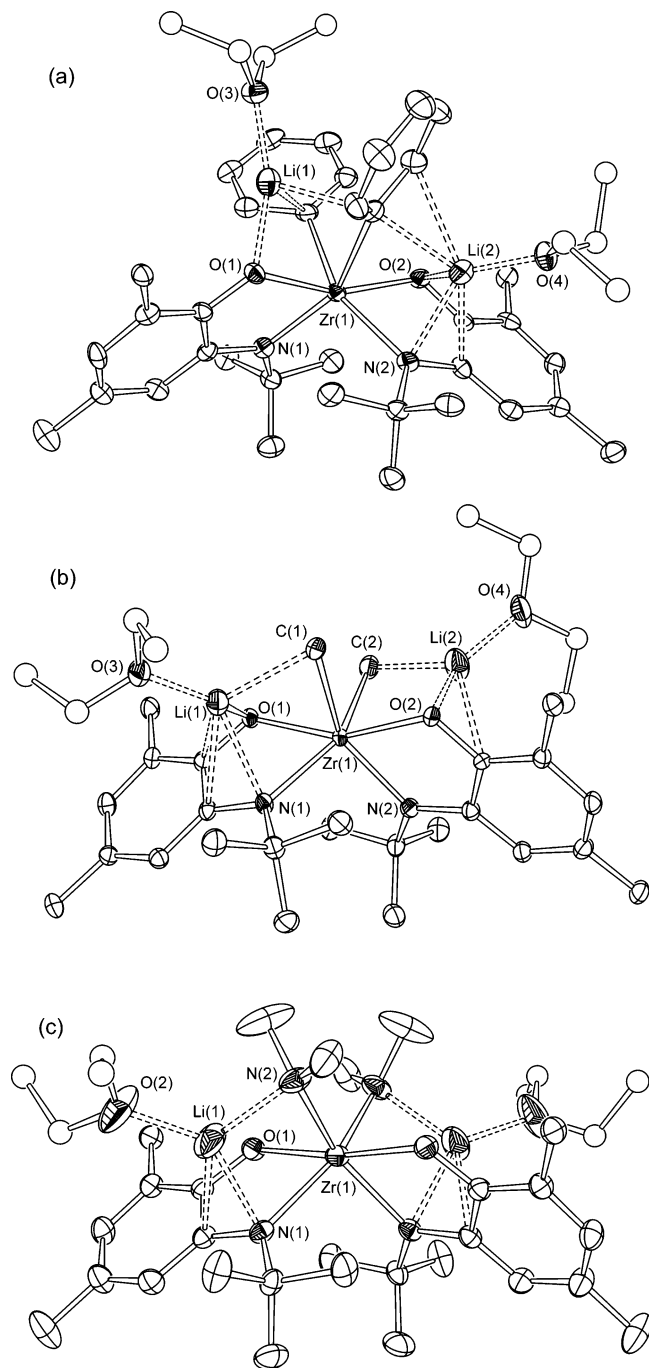
Figure 1. ORTEP diagrams of (a) [Li(OEt₂)]₂[ZrPh₂(ap)₂] (**3a**), (b) [Li-(OEt₂)]₂[ZrMe₂(ap)₂] (**4**), and (c) [Li(OEt₂)]₂[Zr(NMe₂)₂(ap)₂] (**5**). Ellipsoids are drawn at 50% probability. For purposes of clarity, diethyl ether carbons are represented as isotropic spheres and hydrogen atoms and methyl carbon atoms of the ap²⁻ ring *tert*-butyl groups have been omitted.

pseudo-octahedral geometry. The X-ray crystal structures of **3a** and **4** have been reported previously; however, for comparison, ORTEP diagrams for these complexes are presented Figure 1 and selected metrical data are presented in Table 2. X-ray quality single crystals of **5** were obtained by cooling a pentane solution of the complex to −35 °C overnight. Unlike **3a** and **4**, compound **5** crystallizes in the orthorhombic *Pbcn* space group with the zirconium atom on a 2-fold rotation axis. The zirconium center in **5** is six-coordinate and distorted less from octahedral geometry than

Table 2. Selected Bond Distances (Å) and Angles (deg) for [Li(OEt₂)]₂[ZrPh₂(ap)₂] (**3a**), [Li(OEt₂)]₂[ZrMe₂(ap)₂] (**4**), and [Li(OEt₂)]₂[Zr(NMe₂)₂(ap)₂] (**5**)

	3a	4	5
Bond Distances/Å			
Zr(1)−X(1)	2.367(4)	2.384(3)	2.204(2)
Zr(1)−X(2)	2.450(4)	2.386(3)	−
Zr(1)−O(1)	2.147(3)	2.1341(16)	2.0863(17)
Zr(1)−O(2)	2.121(3)	2.1359(17)	−
Zr(1)−N(1)	2.146(3)	2.239(2)	2.285(2)
Zr(1)−N(2)	2.241(3)	2.193(2)	−
X(1)···X(2)	3.324	3.439	3.310
Bond Angles/deg			
X(1)−Zr(1)−X(2)	87.30(13)	92.71(10)	97.14(14)
X(1)−Zr(1)−O(1)	88.74(12)	86.25(8)	89.31(7)
X(1)−Zr(1)−N(1)	90.56(13)	92.20(10)	88.35(9)
O(1)−Zr(1)−O(2)	159.46(10)	157.29(6)	171.53(9)
N(1)−Zr(1)−N(2)	104.55(12)	100.11(8)	96.19(10)

was observed for **3a** and **4**. For example, the O−Zr−O angle in bis(dimethylamide) complex **5** is 171.53(9)°, whereas the same angle in **3a** and **4** is less than 160°. Similarly, the N−Zr−N angle of 96.19(10)° between the cis ap²⁻ nitrogen donors of **5** is significantly smaller than it is in **3a** and **4**. The ap²⁻ ligand in **5** binds with a short Zr−O bond and a long Zr−N bond relative to the distances observed in complexes **3a** and **4**. It is also noteworthy that the bond distance between the zirconium and the dimethylamide nitrogen atoms is relatively short at 2.204(2) Å. Because the strong π-donor dimethylamide ligands are located trans to the ap²⁻ nitrogen donor atoms, competition for the same metal-centered σ- and π-symmetry orbitals may result in longer bonds to the ap²⁻ nitrogens. Supporting the idea that the dimethylamide ligands act as π donors to the metal center is planarity of the amide nitrogen. The sum of the angles around this amide nitrogen is 349.8°, consistent with sp² hybridization.

Two lithium-etherate cations are coordinated to each six-coordinate zirconium complex. Each lithium ion bridges between one dimethylamide ligand and one ap²⁻ ligand. As seen in Figure 1, a similar coordination mode is observed for the lithium-etherate in dimethyl complex **4** but not in diphenyl complex **3a**. In this latter case, the lithium-etherate cations are coordinated unsymmetrically. One lithium-etherate cation bridges between the two phenyl ligands and an ap²⁻ ligand while the second bridges between a phenyl ligand and the other ap²⁻ ligand. It appears that the lithium-etherate cation that bridges the two phenyl ligands also holds them together: despite long Zr−C bond distances in **3a**, the nonbonding C···C distance is short at 3.324 Å, owing to an acute C−Zr−C angle of 87.30°.

Behavior of Zirconium Amidophenolate Dianions in Solution. In benzene-*d₆* solution, complexes **3**−**5** display ¹H and ¹³C NMR spectra consistent with their solid-state structures.[16] The ¹H NMR spectra of **3a**, **4**, and **5** show sharp peaks consistent with nominal *C₂* symmetry in solution: three different ᵗBu groups and two different aryl protons are observed for the equivalent ap²⁻ ligands. The ¹H NMR spectra of **3**−**5** also show sharp ¹H NMR resonances for the

(16) Tabulated ¹H and ¹³C NMR data for complexes **3a**, **3b**, **4**, and **5** in benzene-*d₆* can be found in the Supporting Information.

lithium-bound ether molecules observed in the solid-state structure. The ^{1}H NMR spectra are distinguished by the resonances for the monodentate anionic ligands of each complex. Three aryl ^{1}H NMR resonances are observed for diphenyl complex **3a** at 6.98, 7.13, and 8.79 ppm for the para, meta, and ortho protons, respectively. A singlet ^{1}H NMR resonance is observed for the methyl ligands of **4** at 0.13 ppm. In the case of **5**, the dimethylamide ligand protons are observed as a sharp singlet resonance at 3.16 ppm, indicating fast rotation about the Zr−N bond.

Whereas the solution NMR spectrum of bis(dimethylamide) complex **5** in benzene is consistent with the solid-state structure, the ^{1}H NMR spectrum of the complex in THF-d_8 solution suggests a fluxional coordination environment. Crystalline samples of **5** that gave rise to a clean ^{1}H NMR spectrum in benzene-d_6 gave rise to a complex ^{1}H NMR spectrum when dissolved in THF-d_8. The aliphatic region of the ^{1}H NMR spectrum of **5** in THF-d_8 shows six peaks assignable as *tert*-butyl groups of ap^{2-} ligands. Similarly, the aromatic region shows two different ap^{2-} ligand environments in unequal ratios. Removal of the THF-d_8 solvent followed by addition of benzene-d_6 regenerated the clean ^{1}H NMR spectrum of **5** (excepting the coordination of THF to the lithium cations). The room temperature ^{1}H NMR data for **5** in THF-d_8 is consistent with an equilibrium ligand dissociation process as shown in eq 1. Relative integration of the ap^{2-} ligand peaks gave K_{eq} = 0.30(5) for the dissociation of lithium dimethylamide from **5** to make five-coordinate mono-amide complex, **6**. The assignment of **6** as a five-coordinate mono-amide complex and the estimated equilibrium constant both are supported further by NMR studies of the reaction of **1** with LiNMe$_2$. Addition of less than 2 equiv of LiNMe$_2$ to **1** yields higher ratios of **6:5**, while the addition of more than 2 equiv of LiNMe$_2$ to **1** drives the equilibrium toward complex **5**.[17]

(1)
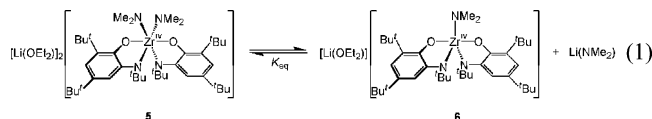
Variable-temperature ^{1}H NMR spectroscopy was used to probe the kinetics of LiNMe$_2$ exchange from **5** in THF-d_8. While the ^{1}H NMR spectrum of crystalline samples of **5** in THF-d_8 showed resonances consistent with the two zirconium species shown in eq 1, when 2 equiv of LiNMe$_2$ was added to the solution, the ^{1}H NMR spectrum simplified to show only the six-coordinate zirconium species. Figure 2 shows ^{1}H NMR spectra, collected at −35, −5, and 25 °C, of complex **5** in THF-d_8 with 2 equiv of free LiNMe$_2$ added to the solution. The 25 °C spectrum is consistent with fast exchange of LiNMe$_2$ bound to the zirconium center and free LiNMe$_2$ in solution. A single resonance for coordinated and free lithium dimethylamide was observed at 2.89 ppm. As

(17) Attempts to isolate pure samples of **6** have been unsuccessful; however, when 1 equiv of LiNMe$_2$ is added to **1** along with 2 equiv of tmeda, the related complex [Li(tmeda)$_2$][Zr^{IV}(NMe$_2$)(ap)$_2$] can be isolated. A preliminary crystal structure confirms the connectivity and geometry proposed in eq 1.
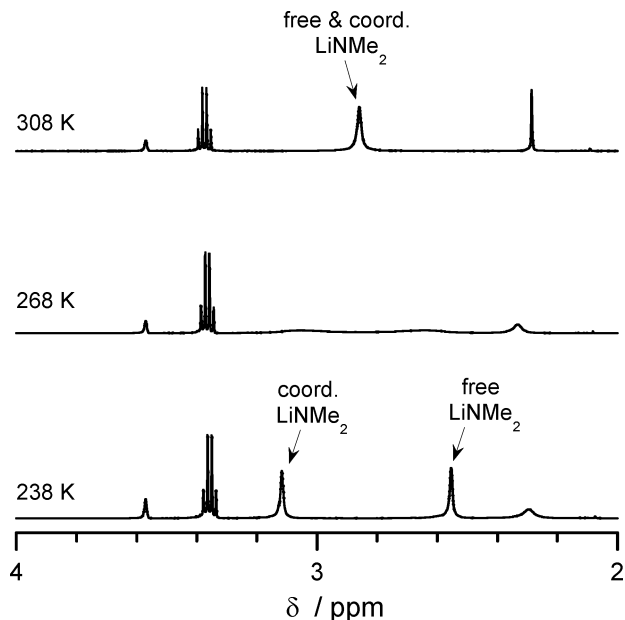
Figure 2. Partial ^{1}H NMR spectra of [Li(OEt$_2$)]$_2$[Zr(NMe$_2$)$_2$(ap)$_2$] (**5**) and 2 equiv of LiNMe$_2$ in THF-d_8 at 238, 268, and 308 K.

Table 3. Measured Rate Constants for the Reactions of [Li(OEt$_2$)]$_2$[ZrX$_2$(ap)$_2$] (**3a**, X = Ph; **4**, X = Me; **5**, X = NMe$_2$) with LiX′ (X′ = *p*-tolyl, CD$_3$, NMe$_2$)

| compound	X′	T/K	k/M^{-1} s^{-1}
3a	*p*-tolyl	298	4.8(7) × 10^{-5}
		308	7.6(36) × 10^{-5}
		318	2.2(4) × 10^{-4}
		328	5.9(16) × 10^{-4}
		338	2.31(3) × 10^{-3}
4	CD$_3$	268	2.1(1) × 10^{-4}
		278	7.0(10) × 10^{-4}
		288	1.7(7) × 10^{-3}
		298	2.6(10) × 10^{-3}
		308	5.6(20) × 10^{-3}
5	NMe$_2$	248	10(3)
		258	5.3(3) × 10^1
		268	2.5(2) × 10^2
		278	1.1(1) × 10^3
		288	3.4(1) × 10^3
		298	1.0(2) × 10^4

the solution was cooled, this singlet broadened and eventually split into two equal-intensity peaks at 3.15 and 2.58 ppm, assignable to two zirconium-bound LiNMe$_2$ ligands and 2 equiv of free LiNMe$_2$ in solution. Under the conditions used to monitor the exchange process (i.e., added LiNMe$_2$), the mono-lithium dimethylamide adduct **6** was not observed. Exchange rate data were obtained from the band shape of the LiNMe$_2$ resonances between −25 and +35 °C. Calculated rate constants are presented in Table 3 (see Supporting Information for observed and calculated spectra) and activation parameters for the exchange process were derived from the Eyring plot shown in Figure 3. Activation parameters of $\Delta H^{\ddagger}$ of 20 kcal mol^{-1} and $\Delta S^{\ddagger}$ of 27 eu are consistent with a dissociative rate-determining step for LiNMe$_2$ exchange, which also is consistent with the proposed equilibrium process shown in eq 1. This conclusion is supported further by concentration-dependence studies of the reaction rate, which displayed a first-order dependence on the concentration of **5** and a zero-order dependence on the concentration of free LiNMe$_2$.
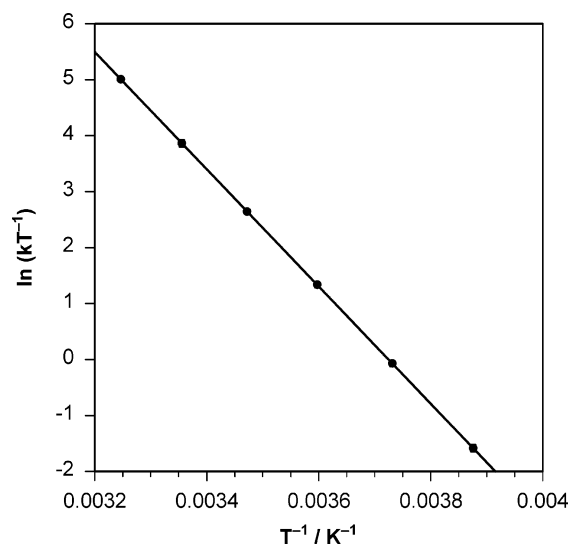
Figure 3. Eyring plot for the exchange of LiNMe$_2$ from **5**. Rate constants were measured by peak coalescence in the ^{1}H NMR spectra of **5** with 2 equiv of free LiNMe$_2$.

Ligand Exchange Kinetics for Dimethyl and Diaryl Zirconium Amidophenolate Dianions. The rapid dissociation of LiNMe$_2$ from **5** prompted an investigation of PhLi and MeLi exchange from complexes **3a** and **4**, respectively. The ^{1}H NMR spectra of **3a** and **4** in THF-d_8 are consistent with the solid-state structures and benzene-d_6 NMR spectra observed for each compound. A single well-defined ligand environment for the ap^{2-} ligands was observed, though in THF-d_8, the ap^{2-} ^{1}H NMR resonances of both **3a** and **4** are shifted to lower frequency. The most dramatic chemical shift difference between benzene-d_6 and THF-d_8 solvents was observed in the zirconium-phenyl resonances of **3a** and the zirconium-methyl resonances of **4**. In the case of **3a**, the three phenyl ligand resonances shift upfield by ca. 0.25 ppm; in the case of **4**, the methyl ligand resonance shifts upfield by 0.5 ppm to -0.45 ppm. Despite these changes in chemical shift, the ^{1}H NMR spectra of **3a** and **4** appeared static at ambient temperature in THF-d_8 with little or no evidence of exchange-based line-broadening in the spectra.

While the exchange of PhLi from **3a** or MeLi from **4** is slow on the NMR time scale, exchange can be observed by ^{1}H NMR spectroscopy using traditional kinetics techniques. Addition of excess p-tolyllithium to THF-d_8 solutions of **3a** resulted in changes to the ^{1}H NMR spectrum consistent with formation of **3b**. Three aromatic proton resonances at 6.79, 6.91, and 8.46 ppm, attributable to the phenyl ligands of **3a** decrease in intensity with concomitant growth of proton resonances at 2.15, 6.75, and 8.35 ppm for the p-tolyl ligands of **3b**. The reaction, shown in eq 2, is completely reversible; independently prepared samples of **3b** reacted with excess PhLi in THF-d_8 to generate **3a**.

(2)
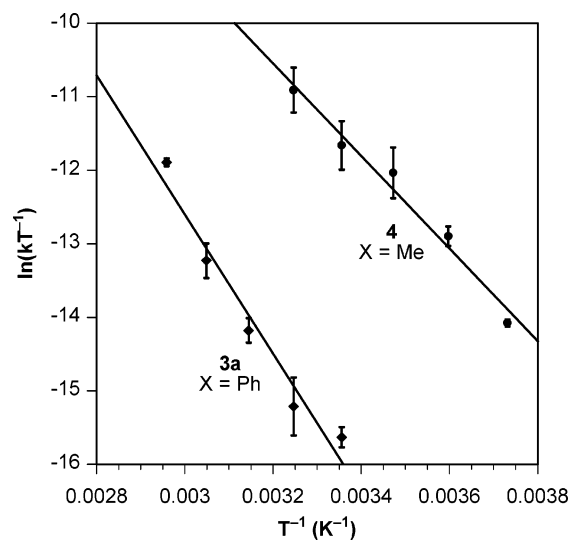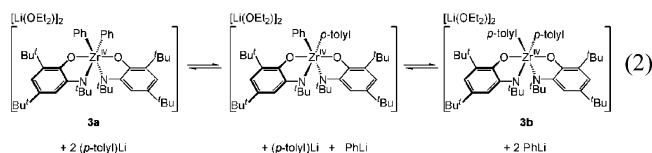
Figure 4. Eyring plot for the exchange of LiX from [Li(OEt$_2$)]$_2$[ZrX$_2$-(ap)$_2$] (**3a**, X = Ph, ♦; **4**, X = Me, ●). Rate constants were measured by the method of initial rates.

Table 4. Kinetic Data for LiX Exchange from [Li(OEt$_2$)]$_2$[ZrX$_2$(ap)$_2$] (**3a**, X = Ph; **4**, X = Me; **5**, X = NMe$_2$)

compound	X	$\Delta H^{\ddagger}$/kcal mol^{-1}	$\Delta S^{\ddagger}$/eu	$\tau_{1/2}$ (298 K)
3a	Ph	19 ± 4	−16 ± 10	4.0 h
4	Me	13 ± 2	−28 ± 7	4.5 min
5	NMe$_2$	20 ± 1	7 ± 3	53 μs

The RLi exchange reaction shown in eq 2 was studied under pseudo-first-order conditions in the presence of excess PhLi and p-tolylLi. In a typical experiment, PhLi exchange was monitored for THF-d_8 solutions of **3a** (10 mM) containing 10 equiv of p-tolyllithium and 8 equiv of phenyllithium. The reactions were monitored by ^{1}H NMR spectroscopy until equilibrium was established. Reactions starting with either **3a** or **3b** do not go to completion, consistent with the exchange of a Zr−phenyl interaction for a Zr−tolyl interaction being thermoneutral. Under these conditions, the exchange processes shown in eq 2 can be modeled as reversible first-order reactions and rate constants can be obtained using eq 3.[18,19] Concentration-dependence studies showed that the approach to equilibrium is first order with respect to the zirconium complex and zero order with respect to the excess PhLi and p-tolylLi reagents. Table 3 shows the measured rate constants determined between 298 and 338 K (see Supporting Information for decay plots); an Eyring plot is shown in Figure 4, and the calculated activation parameters are presented in Table 4.

$$[5]_t = [5]_{eq} + ([5]_0 - [5]_{eq})e^{-(k_1 + k_{-1})t} \qquad (3)$$

MeLi exchange from **4** also was monitored by ^{1}H NMR spectroscopy using the same kinetic techniques. In experi-

(18) Espenson, J. H. *Chemical Kinetics and Reaction Mechanisms*, 2nd ed.; McGraw-Hill, Inc.: New York, 2002; Chapter 3.

(19) Under the conditions used, ^{1}H NMR spectroscopy was used to monitor the number of total number of Zr−Ph and Zr-p-tolyl groups. We had to assume that the rate of exchange of a PhLi for a p-tolylLi was independent of whether the neighboring group was PhLi or p-tolylLi. Since very similar rate constants were obtained for the forward and reverse reactions, this is a valid assumption.

ments analogous to those experiments described above for **3a**, the addition of excess CH₃Li and CD₃Li to THF-d_8 solutions of **4** resulted in the decay of the Zr−CH₃ resonance at −0.45 ppm and the appearance of a new resonance for uncoordinated MeLi at −2.0 ppm, consistent with the exchange of CH₃Li for CD₃Li as shown in eq 4. Under the experimental conditions, the reaction came to equilibrium with [Zr−CH₃] ≈ [Zr−CD₃]. Concentration-dependence studies show that the exchange process is first-order in **4** and zero-order in both CH₃Li and CD₃Li. The reaction rate constants shown in Table 3 were determined by monitoring the ¹H NMR spectrum for mixtures as they approached equilibrium (see Supporting Information for decay plots). An Eyring plot summarizing the temperature-dependence of the exchange rate between 268 and 308 K is shown in Figure 4; calculated activation parameters for the exchange process are presented in Table 4.
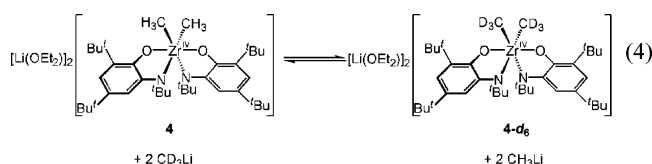
Discussion

Six-coordinate, dianionic complexes of the Group IV metals have received considerable attention both experimentally and theoretically, since simple ligand-field arguments cannot be applied to predict or rationalize coordination geometry.[20−28] Tris-catecholate complexes of titanium are well known, and these species usually adopt a pseudo-octahedral geometry.[29] These tris-catecholate complexes are very stable, for example, simple catechol and its ring-substituted congeners react rapidly with TiCl₄ in aqueous HCl solutions to form the homoleptic complex [Ti(cat)₃]²⁻. This species is stable in acidic water and has been used to great effect as an anchor point in the construction of metal−organic supramolecular assemblies, owing to the robust binding of all three catecholate ligands.[30] In contrast to the

stability of the tris-catecholate titanium(IV) dianions, hexa-alkyl and hexa-amide dianions of zirconium are known to be fluxional in solution. Lithium amide dissociates from Chisholm's [Li(OEt₂)]₂[Zr(NMe₂)₆] complexes on the NMR time scale in a toluene solution,[31] and Girolami's [Li-(tmeda)]₂[ZrMe₆] complex is stable only when tmeda is available to sequester and stabilize the lithium ion.[32] By utilizing substitutionally stable catecholate ligands, it was possible to examine the exchange processes of monodentate, anionic aryl, methyl, and amide ligands.

The stability of the Zr(ap)₂ core provides a useful platform for studying the exchange dynamics of monodentate, anionic donor ligands from **3a**, **4**, and **5**. Under the conditions used in the studies reported here, there is no evidence for the exchange of an ap²⁻ ligand from **3a**, **4**, and **5**, nor have we observed formation of tris(amidophenolate) complexes, [Zr(ap)₃]²⁻. While solutions of dimethylamide complex **5** in benzene-d_6 display straightforward NMR spectra, in the coordinating solvent THF-d_8, an equilibrium mixture of **5** and **6** is observed as shown in eq 1. In the presence of 2 equiv of LiNMe₂, the equilibrium is forced to the left, but the exchange of coordinated and free LiNMe₂ is suitably fast to allow kinetic measurements by variable temperature ¹H NMR spectroscopy. The full rate law for the equilibrium shown in eq 1 is given in eq 5.

$$\text{rate} = k_1[\mathbf{5}] - k_{-1}[\mathbf{6}][\text{LiNMe}_2] \qquad (5)$$

Since the measured exchange rate for **5** is independent of [LiNMe₂], the capture of five-coordinate **6** by free LiNMe₂ must be fast in the presence of excess LiNMe₂ and the forward component of eq 5 dominates the rate law. At equilibrium, the rate constant for the second-order capture of **6** by free LiNMe₂ can be obtained from K_{eq} and k_1 (eq 5)

$$k_{-1} = \frac{k_1}{K_{eq}} \qquad (6)$$

giving a value of $k_{-1} = 4 \times 10^4$ mol⁻¹ s⁻¹ at 298 K. The observation of both species in THF-d_8 and the conversion of this mixture to pure **5** upon addition of excess LiNMe₂ allows us to approximate both the ground-state and transition-state free energies relating the six- and five-coordinate zirconium species: $\Delta G°(298\ \text{K}) \approx 0.6$ kcal mol⁻¹ and $\Delta G^{\ddagger}$-(298 K) = 12 kcal mol⁻¹.

The exchange of PhLi and MeLi from **3a** and **4**, respectively, is considerably slower than the exchange of LiNMe₂ from **5**, yet kinetic experiments suggest that exchange still occurs by a dissociative mechanism. Initial-rate experiments with varied concentrations of LiX (X = Ph, p-tolyl, Me, CD₃) showed no rate dependence on free LiX in solution. There was no direct evidence for LiX aggregation effects under the conditions used. Experiments with added LiBPh₄ did not result in a measureable difference in the LiX exchange rate. The exchange reactions of **3a** and **4** were studied under

(20) (a) Demolliens, A.; Jean, Y.; Eisenstein, O. *Organometallics* **1986**, *5*, 1457−1464; (b) Kang, S. K.; Albright, T. A.; Eisenstein, O. *Inorg. Chem.* **1989**, *28*, 1611−1613; (c) Kang, S. K.; Tang, H.; Albright, T. A. *J. Am. Chem. Soc.* **1993**, *115*, 1971−1981.
(21) (a) Kaupp, M. *J. Am. Chem. Soc.* **1996**, *118*, 3018−3024; (b) Kaupp, M. *Chem. Eur. J.* **1998**, *4*, 1678−1686; (c) Kaupp, M. *Angew. Chem., Int. Ed.* **1999**, *38*, 3034−3037.
(22) Kawaguchi, H.; Tatsumi, K.; Cramer, R. E. *Inorg. Chem.* **1996**, *35*, 4391−4395.
(23) (a) Pfennig, V.; Seppelt, K. *Science* **1996**, *271*, 626−628; (b) Roessler, B.; Pfennig, V.; Seppelt, K. *Chem. Eur. J.* **2001**, *7*, 3652−3656.
(24) Vaid, T. P.; Veige, A. S.; Lobkovsky, E. B.; Glassey, W. V.; Wolczanski, P. T.; Liable-Sands, L. M.; Rheingold, A. L.; Cundari, T. R. *J. Am. Chem. Soc.* **1998**, *120*, 10067−10079.
(25) McGrady, G. S.; Downs, A. J. *Coord. Chem. Rev.* **2000**, *197*, 95−124.
(26) Friese, J. C.; Krol, A.; Puke, C.; Kirschbaum, K.; Giolando, D. M. *Inorg. Chem.* **2000**, *39*, 1496−1500.
(27) Wang, X. F.; Andrews, L. *J. Am. Chem. Soc.* **2002**, *124*, 5636−5637.
(28) Davis, A. V.; Firman, T. K.; Hay, B. P.; Raymond, K. N. *J. Am. Chem. Soc.* **2006**, *128*, 9484−9496.
(29) Borgias, B. A.; Cooper, S. R.; Koh, Y. B.; Raymond, K. N. *Inorg. Chem.* **1984**, *23*, 1009−1016.
(30) Caulder, D. L.; Raymond, K. N. *Acc. Chem. Res.* **1999**, *32*, 975−982.
(31) Chisholm, M. H.; Hammond, C. E.; Huffman, J. C. *Polyhedron* **1988**, *7*, 2515−2520.
(32) Morse, P. M.; Girolami, G. S. *J. Am. Chem. Soc.* **1989**, *111*, 4114−4116.

pseudo-first-order conditions until the systems came to equilibrium. At extended reaction times the exchange reactions for both **3a** and **4** reach equilibrium with $K_{eq} \approx 1$. The observed kinetic data again suggest a first-order rate law and are consistent with a dissociative exchange pathway in which [Li(OEt$_2$)]$_2$[ZrX$_2$(ap)$_2$] loses LiX to form a five-coordinate zirconium species. In the case of complexes **3a** and **4**, the related five-coordinate zirconium complexes were not observed in solution,[33] making equilibrium measurements impossible, but the transition state energies for exchange are considerably higher than that measured for **5**. For **3a**, $\Delta G^{\ddagger}$ (298 K) = 24 kcal mol^{-1}, and for **4**, $\Delta G^{\ddagger}$ (298 K) = 21 kcal mol^{-1}.

The large difference between the LiX exchange rates for **5** (X = NMe$_2$) and for **3a** and **4** (X = Ph and Me, respectively) can be attributed to electronic differences between the X$^-$ groups. Simple electron counting arguments suggest that complex **5** has greater electron density at the zirconium center. Each ap^{2-} ligand is either a four-electron σ donor (2σ(O) + 2σ(N)) or a six-electron donor if π donation is included (2σ(O) + 2σ(N) + 2π).[34] Thus, in the cases of complexes **3a** and **4**, the phenyl and methyl ligands, respectively, act as two-electron donors to the metal center giving 16-electron counts at each zirconium center. Dissociation of a phenyl from **3a** or a methyl from **4** then leaves a five-coordinate species with a maximum electron count of 14. Conversely, in the case of **5**, each dimethylamide ligand can act either as a two-electron donor (2σ only) or as a four-electron donor (2σ + 2π) to the zirconium center. As such, the loss of a dimethylamide ligand from **5** leaves five-coordinate **6**, which can still be considered a 16-electron metal center.

Close inspection of the activation parameters for the LiX exchange reactions suggests a change in the rate-determining step between fast-exchanging **5** and slow-exchanging **3a** and **4**. Table 4 summarizes the activation enthalpy and entropy values for the exchange of LiX from **3a**, **4**, and **5**. Complex **5** shows a large and positive $\Delta S^{\ddagger}$ value, consistent with the dissociation of LiNMe$_2$ in the rate-determining step. On the other hand, complexes **3a** and **4** show negative $\Delta S^{\ddagger}$ values, which are inconsistent with a dissociative rate-determining step.[35,36] Whereas associative exchange of anionic silyl ligands has been observed for low-coordinate zirconium complexes,[37] as discussed above, a rate-determining associative attack of LiX on **3a** or **4** can be ruled out on the basis of the concentration-dependence studies. Similarly, a rate-

determining attack by [Li(THF)$_4$]$^+$ cations can be ruled out based on experiments with added LiBPh$_4$. No measurable difference was observed in the reaction rates, indicating that the concentration of free [Li(THF)$_4$]$^+$ in solution does not appear in the experimental rate law.

One associative rate-determining step that is invisible to our kinetics experiments would be a solvent-assisted step. The nature of organolithium reagents in coordinating and non-coordinating solvents has received considerable attention for its importance in the synthesis of complex organic molecules.[38] In THF, organolithium reagents are known to exist as a mixture of several stoichiometric clusters, including RLi(THF)$_2$ and [RLi(THF)]$_2$ along with higher molecularity clusters.[39–42] Given the nature of RLi in THF solution, it seems possible that RLi dissociation from **3a** or **4** is preceded by attack of THF solvent. Such a solvent-assisted, rate-determining step, which would be expected to show a negative value for activation entropy, is consistent with the observed activation parameters. Moreover, under the conditions of our experiment, the solvent dependence in the reaction rate law would be invisible. Further qualitative evidence for the importance of solvent effects in the dissociation of LiX from **3a** and **4** comes from the solution behavior of these complexes in benzene solution. The addition of *p*-tolyllithium or CD$_3$Li to benzene solutions of **3a** or **4**, respectively, does not result in significant organolithium exchange. The lack of LiX exchange is likely due to the decreased ability of benzene to solvate LiX away from the zirconium center. These data suggest that rate-determining THF attack on zirconium-coordinated LiX likely precedes dissociation for **3a** and **4**.

Conclusions

The primary goal of this work has been to understand the dynamic behavior of dianionic zirconium(IV) complexes with redox-active amidophenolate ligands. The redox activity of these ligands has enabled us to realize C−C bond-forming reductive elimination in the specific case of biphenyl elimination upon oxidation of **3a**. While we were keen to compare the kinetic and thermodynamic differences associated with the elimination of differently hybridized C−C bonds, as well as N−N bonds and even C−N bonds, competing free radical reactions prevented the realization of clean reductive elimination reactions for these other bond-forming reactions. Even in the case of oxidation-induced biphenyl elimination from **3a**, biphenyl yields of 75% probably reflect the relative rate of the two-electron oxidation

(33) Five-coordinate [Li(tmeda)$_2$][Zr^{IV}Me(ap)$_2$] has been isolated, and a preliminary crystal structure reveals a pseudo-trigonal bipyramidal zirconium center; however, solution NMR spectra of these crystals dissolved in THF-d$_8$ are broadened into the baseline, even at −35 °C.
(34) While symmetry allows for the ap^{2-} ligand to be considered a 4π (or even a 6π!) electron donor, such electron counting would require the assignment of very unrealistic formal charges to the amidophenolate ligand.
(35) While the interpretation of activation entropies can be dubious, in this case, the similarity of the LiX exchange reaction and experimental conditions and the magnitude of the difference in $\Delta S^{\ddagger}$ values allow for the use of these measured values to answer (or rather raise) mechanistic questions. See ref 34.
(36) Jordan, R. B. *Reaction Mechanisms of Inorganic and Organometallic Systems*; Oxford University Press: New York, 1998.

(37) (a) Wu, Z.; Diminnie, J. B.; Xue, Z. *J. Am. Chem. Soc.* **1999**, *121*, 4300−4301. (b) Yu, X.; Cai, H.; Guzei, I. A.; Xue, Z. *J. Am. Chem. Soc.* **2004**, *126*, 4472−4473. (c) Qiu, H.; Cai, H.; Woods, J. B.; Wu, Z.; Chen, T.; Yu, X.; Xue, Z. *Organometallics* **2005**, *24*, 4190−4197.
(38) Collum, D. B.; McNeil, A. J.; Ramirez, A. *Angew. Chem., Int. Ed.* **2007**, *46*, 3002−3017.
(39) Seebach, D.; Hässig, R.; Gabriel, J. *Helv. Chim. Acta* **1983**, *66*, 308−337.
(40) Bauer, W.; Winchester, W. R.; von Rague Schleyer, P. *Organometallics* **1987**, *6*, 2371−2379.
(41) Eppers, O.; Günther, H. *Helv. Chim. Acta* **1992**, *75*, 2553−2562.
(42) Reich, H. J.; Green, D. P.; Medina, M. A.; Goldenberg, W. S.; Gudmundsson, B. O.; Dykstra, R. R.; Phillips, N. H. *J. Am. Chem. Soc.* **1998**, *120*, 7201−7210.

step to the PhLi exchange reaction reported here. These studies highlight the surprising impact of LiX exchange reactivity that can complicate and even short-circuit such a bond-forming strategy.

Several mechanisms to slow or stop LiX exchange from the $[ZrX_2(ap)_2]^{2-}$ platform can be envisioned. While the strong solvent-dependence of LiX exchange may be exploited, it should be noted that while biphenyl reductive elimination from **3a** as shown in Scheme 1 works well in THF, the reaction is problematic in low-dielectric benzene solvent, presumably due to the low solubility of the oxidants in benzene. Other alternative strategies to circumvent LiX dissociation include cation exchange reactions to substitute heavier alkali metals for the strongly coordinating lithium ion and tethering together the reductive elimination pairs so that the chelate effect stops LiX dissociation. This latter strategy is attractive in that it would present a new method for C−N or C−O reductive elimination to form new heteroatom-substituted ring structures, especially those with difficult to synthesize ring sizes.

Supporting Information Available: Tabulated ^{1}H and ^{13}C NMR data for **3a,b**, **4**, and **5** in both THF-d_8 and benzene-d_6 solvents, full crystallographic table for **5**, as well as a CIF file, and plots of kinetics data used for extracting the temperature-dependence of the rate constants in the LiX exchange reactions of **3a**, **4**, and **5**. This material is available free of charge via the Internet at http://pubs.acs.org.

IC701112X